Model of a source-driven plasma interacting with a wall in an oblique magnetic field

E. Ahedo[a)] and D. Carralero[b)]
E.T.S. Ingenieros Aeronáuticos, Universidad Politécnica de Madrid, Madrid 28040, Spain

A fluid model of a magnetized source-driven plasma is discussed for regimes with (Debye length) ≪ (ion Larmor radius) ≪ (plasma size and collisional mean-free path). Plasma collection by the wall is determined in terms of angle of incidence, magnetic strength, and plasma collisionality. For nonparallel incidence, a three-scale asymptotic analysis reveals a three-region matched structure consisting of a magnetically aligned bulk region, the Chodura layer, and the Debye sheath. Sonic Chodura and Bohm conditions define the singular region transitions. For near-parallel incidence, a separate analysis demonstrates the presence of a diffusive-collisional bulk region followed by a thin collisionless layer, which differs partially from the Chodura layer. A parametric analysis unveils the presence of four regimes depending on plasma collisionality: (1) a collisionless regime, with the magnetically channeled bulk region governed by plasma production; (2) a resistive semicollisional regime, where collisions retard the plasma transport in the bulk region; (3) a diffusive semicollisional regime, where the $E \times B$ drift dominates the ion flux in the bulk region; and (4) a collisional regime, where collisions cancel out magnetic effects. At grazing incidence, plasma collection is found to vary nonmonotonically with plasma collisionality. Nonzero Debye-length effects are discussed briefly. © *2009 American Institute of Physics*.
[DOI: 10.1063/1.3119687]

I. INTRODUCTION

The interaction of a small Debye-length plasma with a material surface in the presence of a strong magnetic field **B** oblique to the surface is a subject of high interest in different areas, such as tokamak plasmas, spacecraft-plasma interaction, and plasma sources. The anisotropy introduced by the oblique magnetic field makes most practical problems three dimensional and almost intractable analytically.

In this context, one dimensional (1D) approaches of the problem are still rich in phenomena because of, on the one hand, the presence of several length scales (such as Debye length, Larmor radii, collisional mean-free paths, and geometrical scales), and, on the other hand, the large influence of the magnetic incidence angle on the plasma response. To this respect, grazing and parallel incidences are the most challenging cases for analysis and, at the same time, have a high practical interest: grazing incidence is favored in tokamak divertors or limiters to reduce the heat flux;[1] near-parallel magnetic fields are applied in helicon plasma sources and in some plasma thrusters.[2,3] Therefore, 1D models are expected to be very valuable in order to understand the qualitative role and interplay of the different phenomena and associated parameters on the plasma response. In addition, the thin layers that form around the surfaces are basically 1D.

The present paper is focused on a planar geometry and magnetized plasmas satisfying the length-scale hierarchy $\lambda_d \ll \lambda_m \ll \lambda_c \sim L$, where λ_d is the Debye length, λ_m is the ion

Larmor radius, λ_c is the collision (i.e., ion friction) mean-free path, and L is the plasma size. The plasma response depends on the angle of incidence of the magnetic field with the wall, ψ, Fig. 1; oblique, grazing, and parallel incidences, defined as $O(1) = \cos \psi < 1$, $\cos \psi \ll 1$, and $\cos \psi = 0$, respectively, will be distinguished. Also, source-driven and source-free planar models are different. In the first case, plasma production (i.e., ionization plus transverse diffusion) introduces the production mean-free path λ_p as an eigenvalue of the problem, and a global plasma balance relates production to the plasma flux collected by the wall.[4] On the contrary, in a source-free (planar) model, the plasma flux to the wall is a dummy constant.

There is a very vast literature for the case of unmagnetized plasmas (i.e., $\lambda_m/L \to \infty$). In the *small Debye-length limit* ($\lambda_d/L \ll 1$) the plasma structure consists of two regions with disparate plasma gradients. An asymptotic two-scale analysis based on taking the formal *zero-Debye-length limit* ($\lambda_d/L \to 0$) in the plasma equations provides much physical insight, by yielding independent descriptions of the bulk quasineutral region and the space-charged Debye sheath, with a well-defined, singular transition between them. The solution of the bulk region depends on geometry, plasma production, and plasma collisionality. On the contrary, the Debye sheath, being planar and collisionless, has a universal solution in terms of the plasma distribution functions. If, far from the wall, the plasma is at rest, the transition condition between the two regions is the sonic Bohm condition, which states that the ion flow is sonic at the sheath entrance.[4,5] In the finite (but nonzero) Debye-length model, the bulk region and the Debye sheath are treated as a single region down to the wall, with no singular transition; then, as long as λ_d/L

a)Electronic mail: eduardo.ahedo@upm.es
b)Present address: Centro de Investigaciones Energéticas, Medioambientales y Tecnológicas (CIEMAT), Madrid 28040, Spain. Electronic mail: daniel.carralero@ciemat.es
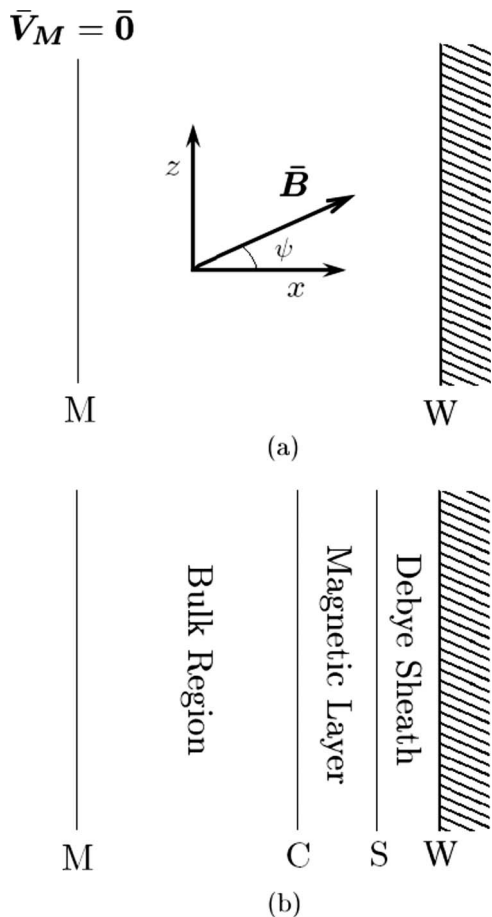
FIG. 1. (a) Geometry of the model. (b) Three-region structure with sonic edges C and S for the zero-Debye-length and zero-Larmor-radius limit.

$\ll 1$, the sonic Bohm condition provides an *approximate* location of the change in the spatial slope in the plasma solution.

Tonks and Langmuir[4] considered a kinetic model for a source-driven, collisionless, unmagnetized plasma in the zero-Debye-length limit (i.e., $\lambda_c/L \to \infty$, $\lambda_m/L \to \infty$, and $\lambda_d/L \to 0$). First, they showed that the resistivity introduced by plasma production in the quasineutral region creates a self-consistent electric field that drives the quasineutral plasma to sonic conditions at the sheath edge. Second, they define the Tonks–Langmuir balance condition, which states that the relation between the sonic Bohm condition and the wall-collected flux determines the plasma production frequency (i.e., the dimensionless parameter λ_p/L) in terms of the rest of model parameters. Fluid formulations of the Tonks–Langmuir model present differences, in main plasma magnitudes, lower than a 10% with respect to the kinetic formulation.[6–8]

Self and Ewald[9] added plasma collisionality to the fluid Tonks–Langmuir model. Collisionless and collisional regimes correspond to $L \ll \lambda_c$ and $\lambda_d \ll \lambda_c \ll L$, respectively. Plasma production (i.e., λ_p/L) depends now on λ_c/L: the additional plasma resistivity caused by ion friction leads to a lower plasma production and a larger potential fall across the plasma. The source-free limit of the Self–Ewald model (i.e., $\lambda_p/L \to \infty$) constitutes indeed a separate model where plasma

collisionality is the only mechanism driving the plasma and the plasma flux is just a dummy parameter.

Turning now to magnetized plasmas, the zero-Debye-length, source-free model (i.e., $\lambda_m/\lambda_c \ll 1$, $\lambda_d/\lambda_m \to 0$, and $\lambda_p/\lambda_c \to \infty$) has been treated by Chodura,[10] Riemann,[11] and Ahedo.[12] Chodura considered the collisionless limit ($\lambda_m/\lambda_c \to 0$) and identified the presence of a double structure, the Chodura–Debye sheath.[10,13] This consists of the classical Debye sheath, preceded by a quasineutral "magnetic presheath" (the *Chodura layer* in the terminology of Ahedo[12]). Their respective length scales are the Debye length and the (ion) Larmor radius. From a time-dependent analysis and postulating the presence of an upstream magnetically aligned bulk region, Chodura found that the magnetically aligned plasma flux must be sonic-supersonic at the upstream edge of the Chodura layer (the general *Chodura condition* in our terminology). At the downstream edge of the Chodura layer (and upstream edge of the Debye sheath) the conventional sonic Bohm condition, asserting that the wall-perpendicular plasma flux is sonic, applies. Thus, the role of the Chodura layer is to drift and accelerate the magnetically aligned ion flux in order it fulfills the sonic Bohm condition. Riemann[11] considered a collisional plasma ($\lambda_m/\lambda_c \neq 0$) and found the quasineutral plasma to consist of a single region that matches directly to the Debye sheath. A connection to the Chodura solution is found for a strong magnetic field ($\lambda_m/\lambda_c \ll 1$), when the main scale length in Riemann´s solution is of the order of the Larmor radius. In a separate analysis of the Chodura layer, Riemann provides a clearer proof of the Chodura condition, based on steady-state equations.

Ahedo[12] reconciles totally the models of Chodura and Riemann by demonstrating that the application of the zero-Debye-length, zero-Larmor-radius, doubly asymptotic limit (i.e., $\lambda_d/\lambda_m \to 0$ and $\lambda_m/\lambda_c \to 0$) to *different* spatial scalings of the plasma equations yields a three-region matched structure, consisting of the magnetically aligned bulk region postulated by Chodura, the Chodura layer, and the Debye sheath, with the sonic Chodura and Bohm conditions defining the singular region transitions. In the small-Larmor-radius limit ($\lambda_m/\lambda_c \ll 1$), the bulk region and the Chodura layer become the single region of Riemann's model; in this case, the Chodura condition provides an *approximate* location of the change of spatial slope in the quasineutral solution (exactly as the sonic Bohm condition does in the small Debye-length limit). Simulations based on the kinetic Boltzmann equation by Devaux and Manfredi[14] confirm (within the tolerances of the nonzero simulation parameters) the three-region plasma structure and their main scalings.

Formally, parallel incidence constitutes a degenerate case of the zero-Larmor-radius limit.[10,11] Ahedo[12] derived a semianalytical matched solution for the source-free case, the quasineutral plasma consisting of a bulk collisional region and a collisionless thin layer. This layer presents resemblances but also some crucial differences with the Chodura layer of oblique incidence, which will be further discussed in the present work.

In a second paper, Riemann[15] extended its zero-Debye-length, finite Larmor-radius model to a source-driven plasma. The plasma structure is similar to the source-free

case but the plasma production frequency is now an eigen-value to be determined. Several recent papers have treated the source-driven model of Riemann. Franklin[16] discussed the Chodura layer (even for the degenerate case of parallel incidence) and the transition between magnetized and un-magnetized responses as λ_m/λ_c goes from small to large. Zimmermannn et al.[17] also analyze the size of the Chodura layer and the evolution of the plasma with λ_m/λ_c; additionally, they discuss a "pseudo-two-scale numerical" procedure to isolate the Chodura layer solution from the bulk region. Sternberg and Poggie[18] focused on the plasma-sheath transition in the small (but nonzero) Debye-length limit. Finally, Sharma and Ramachandran[19] proposed an alternative fluid model to the conventional one of Riemann, but two central elements of their "nonconventional" model are at odds with well-established knowledge. First, their particle and momentum equations for ions contradict the conservation equations derived directly from integral moments of the Boltzmann equation. Second, they claim that (within the zero-Debye-length limit) the standard Bohm condition at the Debye sheath edge is violated generally for a magnetized, source-driven plasma.

This paper adopts the source-driven plasma model of Riemann.[15] Since he already showed that the numerical integration of the equations is straightforward, the work here is centered in several asymptotic studies, aimed at obtaining the three-region plasma structure, both at oblique incidence and near-parallel incidence, and identifying the different regimes of a magnetized plasma. Section II formulates the model. Section III is centered in the application of the zero-Debye-length, zero-Larmor-radius doubly asymptotic limit of Ahedo to the source-driven model and oblique incidence. This will yield again a three-region matched structure with sonic Chodura and Bohm conditions defining the singular entrances of the Chodura and Debye layers, respectively. Section IV derives the three-region solution for near-parallel incidence at the small-Larmor-radius limit and discusses the differences with the solution for oblique incidence. Section V completes the study by matching parametrically the solutions of oblique and near-parallel incidences. In contrast to most previous works, plasma regimes will be presented in terms of input parameters ψ, λ_m/λ_c, and L/λ_c, leaving L/λ_p as the output parameter. Depending on plasma collisionality and apart from the obvious collisional regime, $\lambda_m/\lambda_c \gg 1$, three magnetized regimes are identified for $\lambda_m/\lambda_c \ll 1$. Section VI is devoted to discussion of an alleged violation of the Chodura condition in a tokamak limiter experiment by Harbour and Loarte,[20] and to comment on nonzero Debye-length effects at grazing incidence; these are further discussed in Appendix. Conclusions are in Sec. VII. A first version of this work was presented in a recent Conference.[21]

II. FORMULATION OF THE MODEL

An incidental difference between simple source-free and source-driven models is that they are formulated for semi-infinite and finite plasmas, respectively. In fact, the source-driven, finite-length case can be formulated as a source plasma confined between two parallel walls (for instance, the
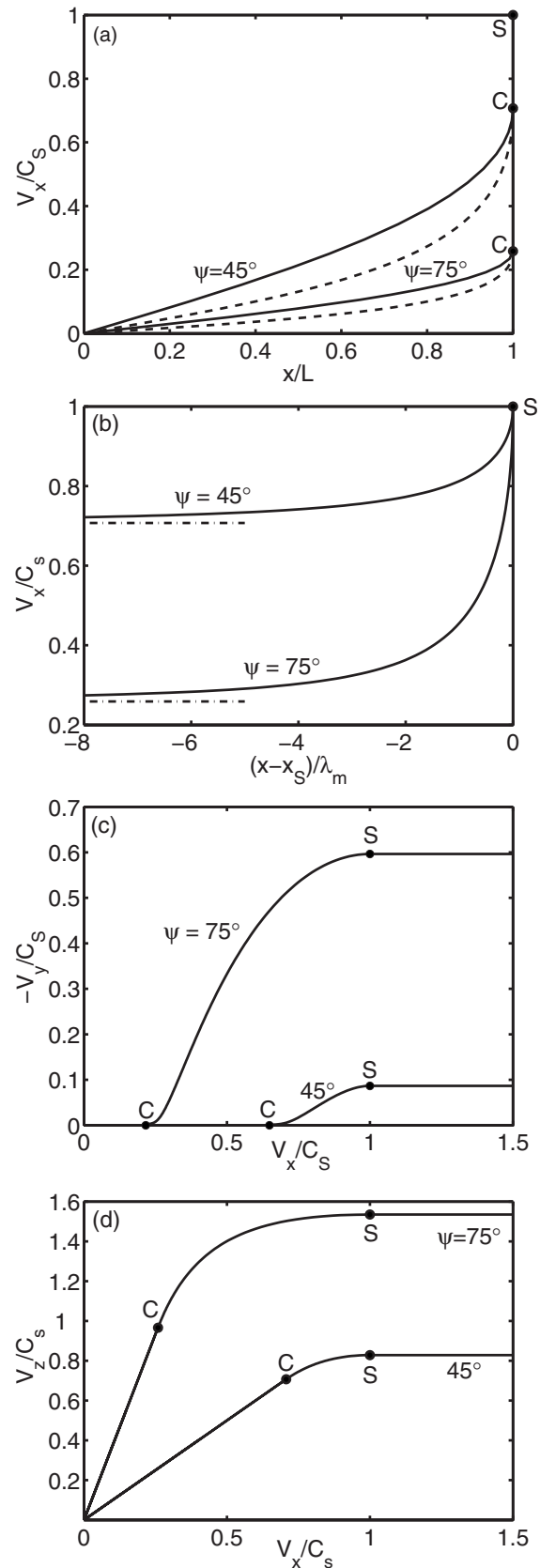

FIG. 2. Zero-Larmor-radius limit for two angles of incidence and two plasma collisionalities: $L/\lambda_c \simeq 0$ (solid lines) and 1(dashed lines). Plasma collisionality affects the bulk region only. [(a) and (b)] Plasma profiles in the bulk region and the Chodura layer, respectively. Dashed-and-dotted lines in (b) mark boundary C. [(c) and (d)] Velocity field behavior with location of edges C and S.

two-wall formulation can be more suitable for numerical simulations, in order to avoid nonphysical sheaths near a no-wall boundary). Thus, let us consider a plasma confined by two parallel, dielectric walls, located at $x = \pm L$ and immersed in an oblique, constant magnetic field,

$$\boldsymbol{B} = B(\boldsymbol{1}_x \cos \psi + \boldsymbol{1}_z \sin \psi),$$

with $0 \le \psi \le \pi/2$, Fig. 1. Plasma properties are uniform in planes $x =$const parallel to the walls, and since the plasma response is symmetric with respect to the channel median M, only the semichannel MW needs to be treated.

For a steady-state response, the plasma satisfies the 1D, macroscopic equations

$$\epsilon_0 \frac{d^2\Phi}{dx^2} = e(N_e - N_i), \tag{1}$$

$$N_e = N_M \exp\frac{e\Phi}{T_e}, \tag{2}$$

$$\frac{d}{dx}(V_x N_i) = N_i \nu_p, \tag{3}$$

$$\frac{d}{dx}(N_i V_x m_i \boldsymbol{V}) = -\boldsymbol{1}_x T_i \frac{dN_i}{dx} - \boldsymbol{1}_x e N_i \frac{d\Phi}{dx} + e N_i \boldsymbol{V} \wedge \boldsymbol{B}$$
$$- \nu_c m_i N_i \boldsymbol{V}. \tag{4}$$

Here Φ is the electric potential, monotonic in each half-channel, and negative if we set $\Phi_M = 0$; N_M is the electron density at the channel median; $\boldsymbol{V}$ is the macroscopic velocity of (singly charged) ions; ν_p is the plasma production frequency (which groups both volumetric ionization and transverse plasma diffusion); ν_c is a momentum-exchange collision frequency for ions (which can also group various contributions); other symbols are conventional.

The momentum-exchange collision frequency for electrons, ν_{ce}, is assumed to satisfy $m_e \nu_{ce} \ll m_i \nu_c$. Then, the electron flux is magnetically aligned and the simple Boltzmann equilibrium law (2), adopted for electrons, applies *except for parallel incidence*. In this work, either "parallel" or "near-parallel" incidence will refer to the formal limit $\psi \to 90°$ (and $m_e / m_i \to 0$) of our model, which is analyzed in Sec. IV. Equations (3) and (4) for particle and momentum fluxes of ions are derived in the standard way from the Boltzmann equation for the ion velocity distribution function. The qualitative, parametric investigation pursued in this work justifies the simple isothermal model for the ion pressure tensor and to take ν_p and ν_c as constant. The source-free model[12] corresponds to Eqs. (1)–(4) with $\nu_p = 0$ and a constant (and dummy) plasma flux, $N_i V_x =$const.

The boundary conditions of the problem are: at the channel median M,

$$N_{iM} = N_M, \quad \boldsymbol{V}_M = \boldsymbol{0}, \quad d\Phi/dx|_M = 0; \tag{5}$$

at the dielectric wall W, the ion and electron fluxes are equal,

$$G_{xiW} = G_{xeW}(\Phi_W), \tag{6}$$

which, indeed, is the condition determining Φ_W. (The extension to other wall conditions is rather straightforward, as long as the walls confine the electrons.)

From Eqs. (3) and (6), the plasma production frequency satisfies

$$\nu_p \int_0^L N_i dx = G_{xeW}, \tag{7}$$

which is the plasma balance condition of the Tonks–Langmuir problem.[4] It asserts that (in steady state) the net plasma production in the channel is equal to the plasma recombination at the walls. Hence, the production frequency, ν_p, is an eigenvalue of the problem.

Let $T = T_e + T_i$ and $C_s = \sqrt{T/m_i}$ be the plasma temperature and sound speed, respectively. The main parameters of the problem are the magnetic incidence angle, ψ, and the following five lengths: the semichannel length, L; the production mean-free-path, $\lambda_p = C_s / \nu_p$; the Larmor radius, $\lambda_m = m_i C_s / eB$; the collision mean-free-path, $\lambda_c = C_s / \nu_c$; and the Debye length at the channel median M, $\lambda_d = \sqrt{\epsilon_0 T / e^2 N_M}$.

Condition (7) implies that λ_p is an eigenvalue of the problem and not a free parameter. Nonetheless, the numerical integration scheme will take λ_p as input parameter and L as eigenvalue.[15] This will determine L/λ_p in terms of ψ, λ_d/λ_p, λ_m/λ_p, and λ_c/λ_p. This relationship is indeed an implicit form of the Tonks–Langmuir balance condition

$$\frac{L}{\lambda_p} = \eta_W\left(\psi, \frac{\lambda_d}{L}, \frac{\lambda_m}{L}, \frac{L}{\lambda_c}\right) \tag{8}$$

in terms of input parameters. The suppression of λ_p in the definition of input parameters is necessary for a proper discussion of the plasma parametric regimes. Similar functional relations apply for the collected plasma flux and other plasma magnitudes. Notice that $L/\lambda_p \equiv \nu_p L / C_s$ and $L/\lambda_c \equiv \nu_c L / C_s$ are dimensionless frequencies for the respective processes.

As stated in Sec. I, the length hierarchy $\lambda_d \ll \lambda_m \ll \lambda_c \sim L$ and the double zero-Debye-length and zero-Larmor-radius formal limit, $\lambda_d/\lambda_m \to 0$ and $\lambda_m/L \to 0$ are adopted as main frame of this work. In contrast, the *small-Larmor-radius* limit[15] keeps λ_m/L nonzero. The *collisionless* limit is defined as $L/\lambda_c \to 0$.

Defining the dimensionless variables

$$\boldsymbol{v} = \boldsymbol{V}/C_s, \quad \phi = e\Phi/T, \quad n_j = N_j/N_M, \quad t_j = T_j/T,$$

with $j = e, i$, the plasma equations become

$$\lambda_d^2 \frac{d^2\phi}{dx^2} = \exp\frac{\phi}{t_e} - n_i, \tag{9}$$

$$\frac{d}{dx}n_i v_x = \frac{n_i}{\lambda_p}, \tag{10}$$

$$v_x \frac{dv_x}{dx} = -\frac{d\phi}{dx} - \frac{t_i}{n_i}\frac{dn_i}{dx} + \frac{v_y \sin \psi}{\lambda_m} - \left(\frac{1}{\lambda_p} + \frac{1}{\lambda_c}\right)v_x, \tag{11}$$

$$v_x \frac{dv_y}{dx} = \frac{v_z \cos\psi - v_x \sin\psi}{\lambda_m} - \left(\frac{1}{\lambda_p} + \frac{1}{\lambda_c}\right)v_y, \tag{12}$$

$$v_x \frac{dv_z}{dx} = -\frac{v_y \cos\psi}{\lambda_m} - \left(\frac{1}{\lambda_p} + \frac{1}{\lambda_c}\right)v_z, \tag{13}$$

where the spatial variable is kept dimensional. The wall-aligned frame is here preferred to the magnetically aligned frame $\{\mathbf{1}_\perp, \mathbf{1}_y, \mathbf{1}_\parallel\}$, with $\mathbf{1}_\perp = \mathbf{1}_x \sin\psi - \mathbf{1}_z \cos\psi$ and $\mathbf{1}_\parallel = \mathbf{1}_x \cos\psi + \mathbf{1}_z \sin\psi$.

Outside the Debye sheath, the quasineutral condition $n_e = n_i \equiv n$ applies and Eqs. (9)–(11) are exchanged by

$$\phi = t_e \ln n, \tag{14}$$

$$\frac{dn}{dx} = \frac{n}{v_x}\left(\frac{1}{\lambda_p} - \frac{dv_x}{dx}\right), \tag{15}$$

$$\left(\frac{1}{v_x} - v_x\right)\frac{dv_x}{dx} = -\frac{v_y \sin\psi}{\lambda_m} + \left(\frac{1}{\lambda_p} + \frac{1}{\lambda_c}\right)v_x + \frac{1}{\lambda_p v_x}. \tag{16}$$

Quasineutral equations are integrated as an initial-value problem from point M, with spatial variable $\eta = x/\lambda_p$. Since conditions (5) make point M a stationary point of the solution, the Taylor expansion of the variables[15]

$$v_x = \eta + O(\eta^3),$$

$$-v_y = \frac{ab \sin\psi}{a^2 + b^2 \cos^2\psi}\eta + O(\eta^3),$$

$$v_z = \frac{b^2 \sin\psi \cos\psi}{a^2 + b^2 \cos^2\psi}\eta + O(\eta^3), \tag{17}$$

$$n = 1 - \frac{a^3 + ab^2}{a^2 + b^2 \cos^2\psi}\eta^2 + O(\eta^4),$$

with $a = 2 + \lambda_p/\lambda_c$ and $b = \lambda_p/\lambda_m$, is needed to define initial integration values at η small. In the $\lambda_d/L \neq 0$ model, the integration ends when the wall condition (6) is satisfied and determines $L/\lambda_p = \eta_W$, Eq. (8).

III. OBLIQUE INCIDENCE

A. The three-region matched structure

We consider $\cos\psi = O(1)$ and the distinguished case $L/\lambda_c = O(1)$, which will yield $\lambda_p \sim L$. Following Ahedo,[12] we apply the zero-Debye-length and zero-Larmor-radius double limit to appropriate dimensionless scalings of the plasma equations.

The equations for the *bulk region* come out from using the spatial variable $\eta = x/\lambda_p$ and taking the asymptotic limit $\lambda_p/\lambda_m = \infty$ in Eqs. (12), (13), and (16). This leads to

$$\frac{\lambda_p}{\lambda_m}v_y = v_x \frac{\sin\psi}{\cos^2\psi}\left(1 + \frac{\lambda_p}{\lambda_c} + \frac{dv_x}{d\eta}\right), \tag{18}$$

$$v_z = v_x \tan\psi, \tag{19}$$

$$\left(1 - \frac{v_x^2}{\cos^2\psi}\right)\frac{dv_x}{d\eta} = \alpha^2 \frac{v_x^2}{\cos^2\psi} + 1, \tag{20}$$

with

$$\alpha^2 = 1 + \lambda_p/\lambda_c.$$

Equation (18) states that $E \times B$ drift v_y goes to zero with the formal limit $\lambda_m/\lambda_p \to 0$. Equation (19) states that the ion flow is magnetically aligned, $\mathbf{v} = v\mathbf{1}_\parallel$ and $v = v_x/\cos\psi$.

Integrating Eqs. (20) and (15), the solutions for $v_x(\eta;\alpha)$ and $n(\eta;\alpha)$ are given implicitly by

$$\frac{\alpha^3 \eta(v_x)}{\cos\psi} = (1 + \alpha^2)\arctan\frac{\alpha v_x}{\cos\psi} - \frac{\alpha v_x}{\cos\psi}, \tag{21}$$

$$n(v_x) = \left(1 + \frac{\alpha^2 v_x^2}{\cos^2\psi}\right)^{-(1+\alpha^2)/(2\alpha^2)}. \tag{22}$$

Collisionless and collisional limits of the magnetically aligned region correspond to the cases $\alpha = 1$ and $\alpha \gg 1$ respectively. Riemann[15] obtained these expressions in a less formal way, applying supplementary approximations on the finite Larmor-radius equations. For normal incidence, the above equations reduce to those of Self and Ewald.[9]

Equation (20) anticipates that the bulk region presents a turning point C at $v_x = v_{xC} = \cos\psi$, with infinite slopes of plasmas variables (except for the plasma flux). This turning point marks the transition to the Chodura layer, with larger spatial gradients and electric fields. Plasma conditions at boundary C are

$$\mathbf{v}_C = (\cos\psi, 0, \sin\psi), \quad n_C = (1 + \alpha^2)^{-(1+\alpha^2)/(2\alpha^2)},$$

$$\phi_{CM} \equiv \phi_M - \phi_C = -\ln n_C. \tag{23}$$

The singular condition defining point C states that the magnetically aligned flow is sonic there, $v_C = 1$. Notice that dimensionless velocities are indeed Mach numbers.

The appropriate spatial variable for the *Chodura layer* is $\zeta = (x - L)/\lambda_m$. Using, first, variable ζ in the quasineutral model, and then, taking the asymptotic limits $\lambda_m/\lambda_c = 0$ and $\lambda_m/\lambda_p = 0$, yields

$$nv_x = n_C \cos\psi, \tag{24}$$

$$v_x^2 + v_y^2 + v_z^2 - 2\ln v_x = 1 - 2\ln\cos\psi, \tag{25}$$

$$(v_x + v_x^{-1})\cos\psi + v_z \sin\psi = 2, \tag{26}$$

$$\frac{d\zeta}{dv_x} = \frac{v_x^2 - 1}{v_x v_y \sin\psi}. \tag{27}$$

Equations (25) and (26) represent the conservation of mechanical energy and plasma momentum along the magnetic field. Condition $v_C = 1$ has been used to set the constants on the right-hand sides. If v_C is kept arbitrary, these equations yield a functional relation $v_y^2 = f(v_x; v_C)$, such that[10,11] $f_C = 0$, $df/dv_x|_C = 0$,

$$\left.\frac{d^2f}{dv_x^2}\right|_C = 2\frac{(1 - v_C \cos \psi)^2(v_C^2 - 1)}{v_C^4 \tan^2 \psi},$$

and a solution for the Chodura layer exists only if $v_C \geq 1$ (i.e., the general Chodura condition). Since a solution of the bulk region exists only for $v_C \leq 1$, the unique, compatible condition is the sonic one, $v_C = 1$.

The integration of Eq. (27) yields $\zeta(v_x)$. For $v_C = 1$, one has $d^3f/dv_x^3|_C = 4(\cos \psi)^{-3}$, and the asymptotic behavior near C is[10]

$$-\zeta + \text{const} \simeq \sin \psi \sqrt{\frac{6 \cos \psi}{v_x - \cos \psi}}. \tag{28}$$

At the other end of the Chodura layer, Eq. (27) indicates that a second turning point S appears at $v_x = 1$, which marks the transition to the Debye sheath. Plasma conditions at the transition edge S are

$$v_{xS} = 1, \quad v_{zS} = 2 \tan(\psi/2), \quad -v_{yS} = \sqrt{\ln \cos^{-2} \psi - v_{zS}^2},$$

$$n_S = n_C \cos \psi, \quad \phi_{SC} = \ln \cos^{-1} \psi. \tag{29}$$

The convenient spatial variable in the *Debye sheath* is $\xi = (x - L)/\lambda_{dS}$ with

$$\lambda_{dS} = \sqrt{\epsilon_0 T/e^2 N_S} \equiv \lambda_d n_S^{-1/2} \tag{30}$$

the local Debye length. Rewriting Eqs. (9)–(13) in terms of ξ, then taking the double asymptotic limit, and carrying out some quadratures, yield the sheath conservation laws

$$\frac{1}{2}\left(\frac{d\phi}{d\xi}\right)^2 = t_e \exp\frac{\phi - \phi_S}{t_e} + \frac{t_i}{v_x} + v_x - 2, \tag{31}$$

$$\frac{v_x^2}{2} + \phi - t_i \ln v_x = \frac{1}{2} + \phi_S, \tag{32}$$

$v_y = v_{yS}$, and $v_z = v_{zS}$. The asymptotic condition $d\phi/d\xi|_S = 0$ and $v_{xS} = 1$ have been applied in Eq. (31). The Bohm condition $v_{xS} \geq 1$, comes out from leaving v_{xS} as a parameter in Eq. (31) and requiring that its right-hand side is non-negative around point S. Therefore, there are strong similarities between the general Chodura and Bohm conditions, even though the first one is derived from a magnetized, quasineutral model and the second one from an unmagnetized, non-neutral one.

The integration of the Debye sheath is standard. For a quasi-Maxwellian distribution of confined electrons, Eq. (6) and the sheath solution, determine the sheath potential fall,

$$\phi_{WS} = \phi_S - \phi_W = \frac{1}{2}\ln\frac{m_i T_e}{2\pi m_e T} \gg 1, \tag{33}$$

which is used as the stop condition when Eq. (31) is integrated numerically from edge S.

This completes the derivation of the three-region matched structure. It demonstrates that the Chodura layer is collisionless and source-free, and, therefore, identical to the one in the source-free model. This disagrees with the opinion of Franklin,[16] who asserts that the neglect of plasma production in Chodura's work is its principal deficiency. Also, the validity of the sonic Chodura and Bohm conditions for any

nonparallel incidence angle in the formal asymptotic limits refutes the assertion of Sharma and Ramachandran.[19]

Since the Chodura–Debye double sheath is source-free, the total potential fall in it can be obtained directly from imposing $(NV_x)_C = G_{xeW}$, yielding

$$\frac{e\Phi_{WC}}{T_e} = \frac{1}{2}\ln\frac{m_i T_e}{2\pi m_e T} + \ln\frac{1}{\cos \psi}, \tag{34}$$

in agreement, of course, with Eqs. (29) and (33). The Debye sheath potential fall is insensitive to ψ, but the potential fall in the Chodura layer increases with the angle of incidence, which is a consequence of the larger increment of kinetic energy along Ox to be applied to the plasma. Surprisingly, Chodura[10] stated that the electric potential fall in the Chodura–Debye sheath, Φ_{WC} is fairly insensitive to the angle of the magnetic field.

In the doubly asymptotic limit, the Chodura and Debye layers are seen as a discontinuity in the scale of the bulk region. Therefore, we can set $L/\lambda_p \equiv \eta_W \simeq \eta_C$, and Eqs. (21) and (22) yield

$$\frac{L}{\lambda_p} = \left(\frac{1 + \alpha^2}{\alpha^3}\arctan \alpha - \frac{1}{\alpha^2}\right)\cos \psi, \tag{35}$$

$$\frac{G_{xW}}{N_M C_s} \equiv n_S = (1 + \alpha^2)^{-(1+\alpha^2)/(2\alpha^2)} \cos \psi. \tag{36}$$

These are implicit expressions for the plasma production, Eq. (8), and the wall-collected flux in terms of incidence angle and plasma collisionality (i.e., $\cos \psi$ and L/λ_c) in the limits $\lambda_d/L \to 0$ and $\lambda_m/L \to 0$. Also, they extend to oblique incidence magnetized plasmas the laws of Self and Ewald.

B. Results and discussion

For $L/\lambda_c \to 0$, plasma acceleration is driven exclusively by plasma production. Figures 2(a) and 2(b) show profiles of $v_x(x)$ in the bulk and Chodura regions in their respective scales; well-known Debye sheath profiles are not plotted. Figures 2(c) and 2(d) depict the relative evolution of the three velocity field components along the three distinguished regions, illustrating the magnetic-drift character of the Chodura layer. The plasma response is the result of the self-consistent electric field, $E = E_x \mathbf{1}_x$, created by the plasma. This monotonic electric field experiences a change of magnitude at each region transition, with typical magnitudes Φ_{CM}/L, Φ_{SC}/λ_m, and Φ_{WS}/λ_d, in the respective regions. Observe that the thickness of each region is constrained by geometry (L) or plasma dynamics (λ_m and λ_d). Incidence angle and plasma collisionality affect mainly the electric potential fall in each region [Eqs. (23), (29), and (33)]. It is physically clear that ion acceleration from $v_{xC} = \cos \psi$ to $v_{xS} = 1$ in the collisionless Chodura layer must be achieved in a distance of the order of the ion Larmor radius, before the ion gyromotion limits the increase of B-perpendicular velocities; the resulting electric field produces a significant $E \times B$ drift velocity and the associated Lorentz force responsible of the B-perpendicular ion acceleration.

Notice that the electron flux does not suffer the B-perpendicular acceleration in the Chodura layer and thus is

magnetically aligned up to the Debye sheath edge S. Since plasma continuity assures that v_x is equal for ions and electrons, a wall-parallel electric current density, $en(v_z - v_x \tan \psi)$, is formed in the Chodura layer. This illustrates the asymmetric responses of the wall-attracted ions and the wall-confined electrons.

In order to compare with the zero-Larmor-radius limit, Fig. 3 plots plasma profiles for small (nonzero) Larmor radii when the quasineutral equations are integrated in a single stage from the channel median M to the Debye sheath edge S, as in Ref. 15. The spatial profiles show a broad quasi magnetically aligned region followed by a thin Chodura-like layer. For $\lambda_m/L \neq 0$ the transition between these two regions is regular (i.e., continuous), and any definition of the transition point C is discretionary somehow. If $v_{xC}=\cos \psi$ is used as definition, then $v_C<1$, as in the simulations of Devaux and Manfredi,[14] and one could claim (incorrectly) the violation of the general Chodura condition; an opposite conclusion is reached if $v_C=1$ is used as definition, yielding $v_{xC}>1$. For $\lambda_m/L=O(1)$, the steep Chodura-like layer disappears, the plasma tends to become unmagnetized, and the response becomes independent of ψ; in other words, it coincides with the one for normal incidence, $\psi=0$.

Devaux and Manfredi[14] and Zimmermann et al.[17] discuss in detail, from the small-Larmor-radius model, the size of the Chodura layer, L_{CS}. It must be observed that there is not an exact value for L_{CS} since, on the one hand, for $\lambda_m/L \neq 0$, there is the unavoidable arbitrariness in the definition of point C, and on the other hand, for $\lambda_m/L=0$ the Chodura layer is a discontinuity in the scale of the bulk region, while it is semi-infinite in its own natural scale. Therefore, the most interesting discussion is on the scaling law of L_{CS} with the incidence angle ψ. Chodura proposed the scaling law $L_{CS}/\lambda_m \propto \sin \psi$, based on the asymptotic behavior near C, Eq. (28), but that scaling does not recover well the behavior for large incidence. Figure 4, based on the zero-Larmor-radius model, shows that the simple fitting law $L_{CS}/\lambda_m \propto \sin \psi \sqrt{\cos \psi}$, also based in Eq. (28), is a better choice for most of the range of incidence angles. For grazing incidence, the behavior of v_{yS}, Eq. (29), suggest the fitting $L_{CS}/\lambda_m \propto |\ln \cos \psi|^{-1/2}$, which agrees well with numerical results.

Figures 5(a) and 5(b) illustrate on the Tonks–Langmuir relationship, Eq. (8), in the zero-Debye-length limit, by showing the plasma production frequency L/λ_p versus incidence angle, magnetic strength, and plasma collisionality. The collected plasma flux is not plotted since curves are identical except for a factor lying between 1.1 and 1.6, as expressions below will justify. The main trends are quite simple: plasma production and wall-collection decreases when any of the parameters ψ, λ_m/L, and L/λ_c increase.

Franklin[16] and Zimmermann et al.[17] have discussed the transition between a magnetized and an unmagnetized regime, as the ion Hall parameter λ_c/λ_m evolves from large to small. Indeed, the present analysis distinguishes three regimes (and a fourth one will come out in Sec. IV). There is, first, the (magnetized) *collisionless regime* for $\lambda_m \ll L_\parallel \ll \lambda_c$, where $L_\parallel = L/\cos \psi$ is the median-to-wall length along the
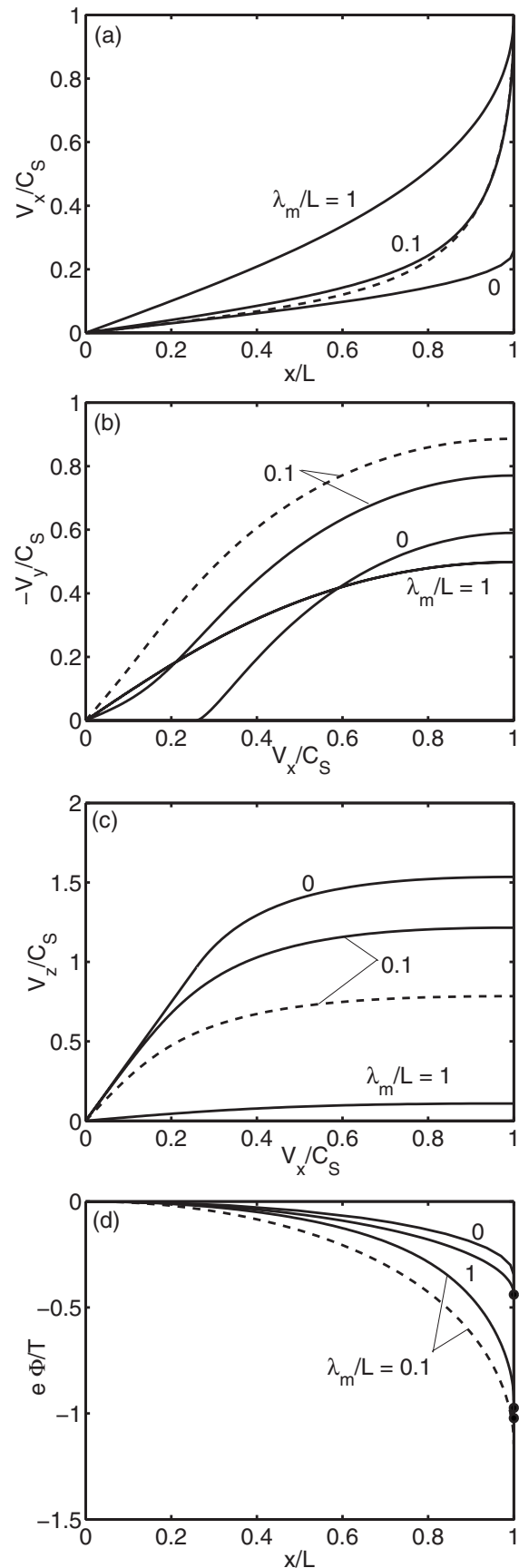

FIG. 3. Finite Larmor-radius model. Quasineutral response for $\psi=75°$ and different magnetic strengths. Continuous lines are for the collisionless limit ($L/\lambda_c=0$). Dashed lines are for the case $L/\lambda_c=1$ and $\lambda_m/L=0.1$. Black points in (d) correspond to edges S of the solid lines (λ_m/L increases from bottom to top).
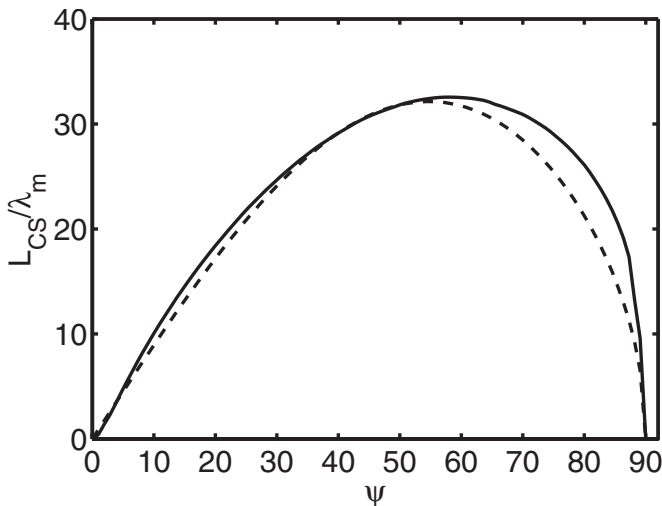
FIG. 4. Scaling of the Chodura layer size with the incidence angle, for the zero-Larmor-radius limit and a collisionless plasma. The layer entrance is approximated as the point where $dv_x/d\zeta = 10^{-4}$; this small derivative explains the large value of L_{CS}/λ_m. Dashed lines correspond to the fitting curve $L_{CS}/\lambda_m \propto \sin\psi\sqrt{\cos\psi}$.

magnetic line. Plasma production and collection, Eqs. (35) and (36), follow the scaling laws

$$n_S \simeq \frac{1}{2}\cos\psi, \quad \frac{L}{\lambda_p} \simeq (\pi-2)n_S \sim 1. \tag{37}$$

Then, there is the (magnetized) *resistive, semicollisional regime* for $\lambda_m \ll \lambda_c \ll L_\parallel$, with production and collection laws

$$n_S \simeq \frac{\pi}{2}\frac{\lambda_c}{L}\cos^2\psi, \quad \frac{L}{\lambda_p} \simeq \frac{\pi}{2}n_S \ll 1. \tag{38}$$

Finally, there is the (unmagnetized) *collisional regime* for $\lambda_c \ll \{\lambda_m, L\}$, with

$$n_S \simeq \frac{\pi}{2}\frac{\lambda_c}{L}, \quad \frac{L}{\lambda_p} \simeq \frac{\pi}{2}n_S \ll 1. \tag{39}$$

The two first regimes are appropriately described by the zero-Larmor-radius limit, where the third one is the well-known solution of Self–Ewald [and corresponds to Eqs. (35) and (36) for $\psi = 0$].

In the transition between the collisionless and the resistive semicollisional regime, the Chodura layer remains unaffected and the bulk region changes from production dominated to friction dominated. As collisionality increases, larger electric fields are created by the quasineutral plasma in order to bring the ion flow to sonic conditions at edge C. This is achieved by incrementing Φ_{CM}, Eq. (23), with the consequences of reducing the collected plasma flux [one has $n_C \propto \exp(-e\Phi_{CM}/T)$] and making $v_x(x)$ more steepened near the wall, as dashed lines in Fig. 2(a) illustrate. The transition between the semicollisional and the collisional regime is characterized by collisionality canceling out all magnetic effects. Thus, the ion flux in the bulk region evolves from being magnetically aligned to wall perpendicular, the Chodura layer vanishes, and the increasing resistivity caused by collisions leads to a lower plasma collection.
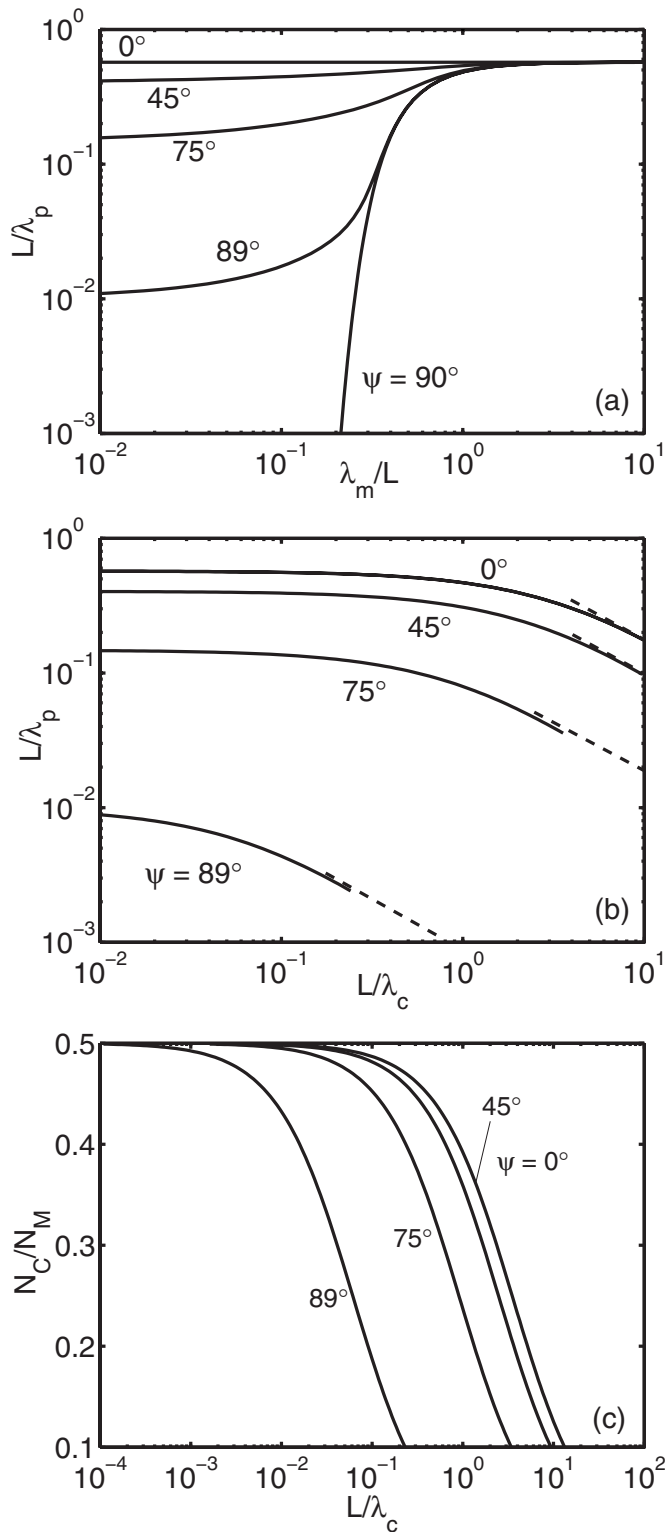

FIG. 5. (a) Plasma production frequency vs magnetic strength for several angles of incidence and a collisionless plasma, $L/\lambda_c = 0$. (b) Plasma production frequency vs plasma collisionality for several angles of incidence, in the zero-Larmor-radius regime; dashed lines correspond to the resistive semicollisional regime. (c) Density at the edge of the Chodura–Debye sheath for same conditions than plot (b).

Observe that the range of L/λ_c defining the collisionless regime decreases as ψ increases and tends to vanish for parallel incidence. Nonetheless, looking at $\psi = 90°$ in Fig. 5(a), it is remarkable that a relatively strong-magnetized plasma

($\lambda_m/L \sim 0.2-0.4$, say) can be accelerated to sonic conditions only by the electric self-field created by plasma-production-based resistivity.

Finally, Fig. 5(c) plots the density at the edge C of the Chodura layer. The upper limit $n_C = 0.5$ corresponds to the collisionless regime. For strongly magnetized plasmas, measurements are not affordable inside the thin Chodura–Debye sheath, so that n_C is the "near-wall" density available from diagnostics.

IV. NEAR-PARALLEL INCIDENCE

The previous analysis provides two important observations when magnetized solutions are extended to near-parallel incidence. First, in the zero-Larmor-radius limit, the three-region structure fails to exist, as in the source-free model.[10,12] Second, for a collisionless plasma and a small-Larmor-radius parameter, plasma production seems to decay exponentially: L/λ_p drops from 7×10^{-4} to 10^{-7} as λ_m/L decreases from just 0.20 and 0.15. This suggests that the adequate frame for studying near-parallel incidence must keep both λ_m/L and L/λ_c as nonzero in the plasma quasineutral equations.

In the formal limit $\psi \to 90°$, the plasma equations for the velocity field become

$$\left(v_x - \frac{1}{v_x}\right)\frac{dv_x}{dx} = \frac{v_y}{\lambda_m} - \left(\frac{1}{\lambda_c} + \frac{1}{\lambda_p}\right)v_x - \frac{1}{\lambda_p v_x}, \tag{40}$$

$$v_x\frac{dv_y}{dx} = -\frac{v_x}{\lambda_m} - \left(\frac{1}{\lambda_c} + \frac{1}{\lambda_p}\right)v_y, \tag{41}$$

and $v_z(z)$ is uncoupled; one has $v_z(z) = 0$ for $v_{zM} = 0$. Numerical solutions of these equations are straightforward. Semianalytical asymptotic solutions for relevant parametric regimes provide more information.

The most distinguished magnetized regime for near-parallel incidence corresponds to

$$\lambda_m \ll \{L, \lambda_c\}, \quad \lambda_c \ll L \exp(L/\lambda_m), \quad \{L, \lambda_c\} \ll \lambda_p, \tag{42}$$

where the second inequality leaves explicitly out the collisionless case, and the last one is an ansatz on λ_p to be confirmed at the end. The quasineutral solution is going to consist of a bulk region and a thin layer. We call D the point locating (approximately) the *regular* transition between them. For $v_x \ll v_{xD} \ll 1$, with v_{xD} to be determined yet, convective terms are negligible in Eqs. (40) and (41), that simplify into

$$\frac{1}{v_x}\frac{dv_x}{dx} \simeq -\frac{v_y}{\lambda_m} + \frac{1}{\lambda_p v_x}, \quad -\frac{v_y}{\lambda_c} \simeq \frac{v_x}{\lambda_m}.$$

Then, the solutions for v_x and n, Eq. (15), are

$$v_x(x) = \frac{\lambda_m}{\sqrt{\lambda_p \lambda_c}}\tan\left(\frac{x}{\lambda_m}\sqrt{\frac{\lambda_c}{\lambda_p}}\right), \tag{43}$$

$$n(x) = \cos\left(\frac{x}{\lambda_m}\sqrt{\frac{\lambda_c}{\lambda_p}}\right). \tag{44}$$

The solution for v_x is valid until the convective term in Eq. (41) becomes significant, that is until $-dv_y/dx \sim 1/\lambda_m$. This allows us to define point D, up to leading order, by

$$x_D \simeq \frac{\pi}{2}\lambda_m\sqrt{\frac{\lambda_p}{\lambda_c}}, \quad n_D \simeq \sqrt{\frac{\lambda_c}{\lambda_p}},$$

$$v_{xD} \simeq \frac{\lambda_m}{\lambda_c}, \quad -v_{yD} \simeq 1. \tag{45}$$

In the region $v_{xD} \ll v_x \leq 1$, production and collisional terms of Eqs. (40) and (41) are negligible. A straightforward integration yields

$$-v_y(x) \simeq (x - x_D)/\lambda_m + a, \tag{46}$$

$$2\ln v_x - v_x^2 = (x - x_D)^2/\lambda_m^2 + 2a(x - x_D)/\lambda_m - 2\ln(b\lambda_c/\lambda_m), \tag{47}$$

$$n = \lambda_m(\lambda_p\lambda_c)^{-1/2}v_x^{-1}, \tag{48}$$

where a and b are constants of $O(1)$ that assure the gentle matching with the region $0 \leq v_x \ll v_{xD}$.

Particularizing Eq. (47) at edge S and keeping only the two dominant terms [for $\ln(\lambda_c/\lambda_m) \gg 1$] one has

$$\frac{L_{DS}}{\lambda_m} \simeq -v_{yS} \simeq \sqrt{2\ln\frac{\lambda_c}{\lambda_m}}, \quad n_S = \frac{\lambda_m}{\sqrt{\lambda_p\lambda_c}}, \tag{49}$$

with $L_{DS} = x_S - x_D$. Except for very low collisionalities, left out by the second condition of Eq. (42), one has $L_{DS} \ll x_D$ and the region DS is a thin layer between the bulk region MD and the Debye sheath. Then, setting $L \simeq x_D$ the scaling laws for plasma production and collection at near-parallel incidence are

$$n_S \simeq \frac{\pi}{2}\frac{\lambda_m^2}{\lambda_c L}, \quad \frac{L}{\lambda_p} \simeq \frac{\pi}{2}n_S, \tag{50}$$

with λ_p satisfying the ansatz made in Eq. (42).

This completes the derivation of the quasineutral solution at near-parallel incidence. It consists of a bulk diffusive-collisional region MD followed by a collisionless thin layer DS with a regular transition at the sonic point D. Figure 6(a)
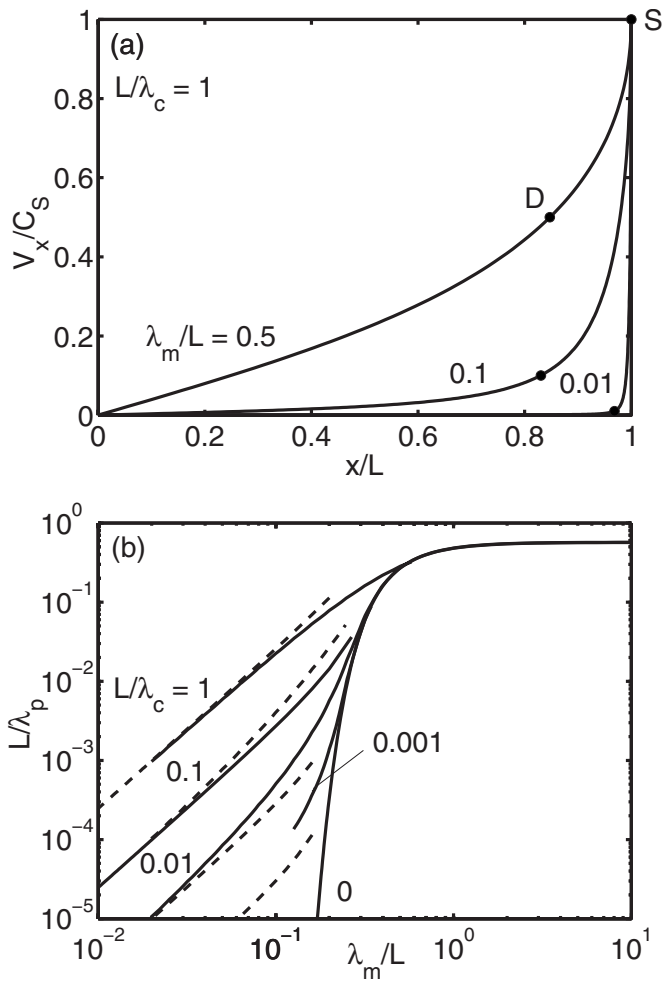
FIG. 6. Near-parallel incidence. (a) Profiles of v_x in the quasineutral region and locations of points D for $L/\lambda_c = 0.1$ and different magnetic strengths. (b) Plasma production vs magnetic strength for different plasma collisionalities; dashed lines correspond to the diffusive semicollisional regime.

plots some profiles illustrating that, for small-Larmor radii, point D is effectively located at the change of slope of the spatial profiles.

The thin layer of this near-parallel, source-driven model is exactly the same obtained by Ahedo for the source-free model[12]; of course, the bulk regions of these two models differ in the functional expressions for $v_x(x)$ and $n(x)$. More interestingly, the comparison between the thin layer of near-parallel incidence and the Chodura layer of oblique incidence yields that they coincide in the following: both are source-free and collisionless, both are governed by convection and magnetic forces based on the $E \times B$ drift, the ion flux is sonic at their entrance, and their thickness scales proportional to the ion Larmor radius. Nonetheless, they present significant differences too. The Chodura layer is preceded by a magnetically aligned bulk region (that can be collisional or collisionless), the $E \times B$ drift develops entirely inside the layer, and the layer size depends on the angle of incidence. The thin layer of near-parallel incidence is preceded by a collisional bulk region, dominated by the $E \times B$ drift and no flow along **B**, and, in spite of being collisionless, its size

depends on plasma collisionality (through the entrance condition v_{xD}).

Figure 6(b) depicts the production frequency as function of λ_m/L and L/λ_c, confirming that Eq. (50) reproduces correctly the asymptotic behavior for small-Larmor radii. The scaling laws of Eq. (50) show that for near-parallel incidence the production frequency and the collected flux decrease quadratically as the magnetic field increases but they *increase linearly* when collisionality increases. This last behavior indicates a diffusive character of collisions for near-parallel incidence, instead of the resistive character for the regimes of oblique incidence. This suggests to name the present regime as *diffusive semicollisional regime*.

Finally, some remarks on the limits of validity of the near-parallel incidence solution are pertinent. On the one hand, it will shown next that this solution extends to incidence angles satisfying $\cos \psi \sim \beta_i^{-1}$ with $\beta_i = \lambda_c/\lambda_m$ the Hall parameter for ions. On the other hand, the Boltzmann equilibrium law Eq. (2) is not a correct model for electrons at $\psi = 90°$, since then B-perpendicular electron transport (supported on collisionality and $E \times B$ drift of electrons) is the only mechanism capable of creating a nonzero electron flux to the wall. A preliminary study on parallel incidence finds that electron perpendicular transport is relevant for $\cos \psi \leq O(\beta_e^{-1/2})$, with $\beta_e = eB/m_e \nu_{ce}$ the electron Hall parameter and ν_{ce} the electron collisionality; we expect $\beta_e \gg \beta_i$. Therefore, the present near-parallel solution (or diffusive semicollisional regime) covers the range $\beta_e^{-1/2} \ll \cos \psi \ll \beta_i^{-1}$.

V. THE THREE MAGNETIZED REGIMES

The extension to $\cos \psi \ll 1$ of the solutions for oblique and near-parallel incidences, provides the desired parametric continuity between them and completes the study. For $\lambda_m \ll \{L, \lambda_c\}$ and $\cos \psi \ll 1$ the plasma is expected to behave in one of the two previous semicollisional regimes. The comparison of scaling laws (38) and (50) for oblique and near-parallel incidences, respectively, shows that, for $\cos \psi \sim \lambda_m/\lambda_c$, they yield similar plasma productions and the definitions of points C and D coincide. Therefore, one expects the diffusive semicollisional (DSC) regime of near-parallel incidence to apply for $\cos \psi \ll \lambda_m/\lambda_c$ (i.e., near-parallel incidence), and the resistive semicollisional (RSC) regime of oblique incidence to be valid for $\cos \psi \gg \lambda_m/\lambda_c$. The numerical solutions of the full equations confirm that parametric transition.

Therefore, for a zero-Debye-length, small-Larmor-radius plasma, there are three magnetized regimes, depending on the incidence angle and the ion collisionality. These are completed by a collisional regime where magnetic effects are canceled out. Asymptotic laws yielding the wall-collected plasma flux in the collisionless, RSC, DSC, and collisional regimes are

FIG. 8. Grazing incidence. Plasma production vs plasma collisionality for $\psi=89°$ and different magnetic strengths. Black points correspond to λ_{c1}, λ_{c2} (minimum), and λ_{c3} (maximum).
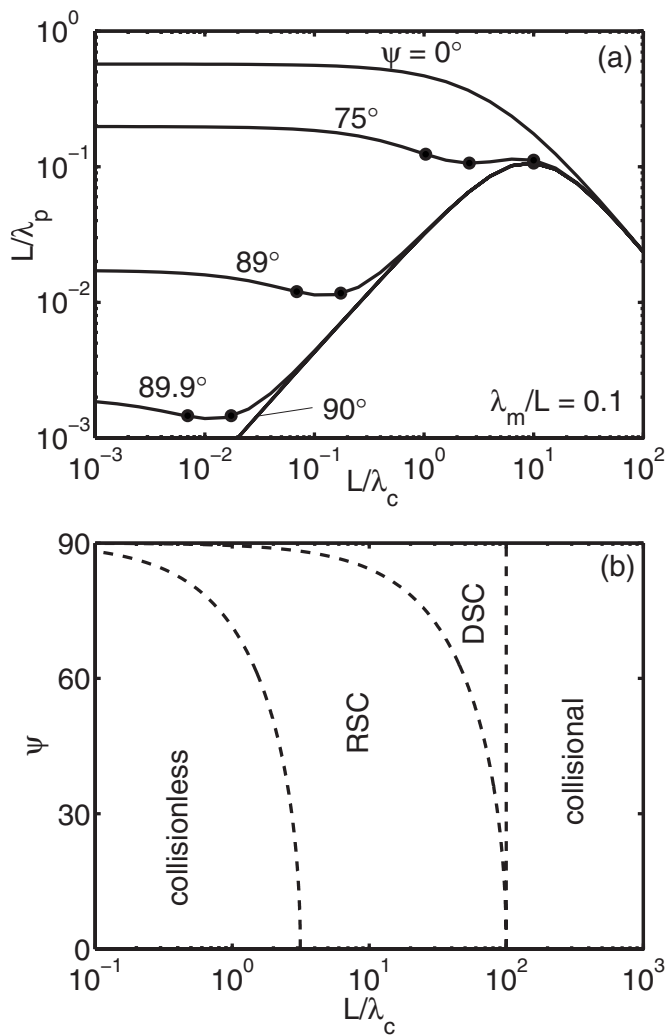

FIG. 7. (a) Plasma production vs plasma collisionality for different angles of incidence and $\lambda_m/L=0.1$; black points correspond (from left to right) to transition values λ_{c1}, λ_{c2} and λ_{c3}. (b) Parametric region in the plane $(L/\lambda_c, \psi)$ of the four operation regimes for a plasma with $\lambda_m/L=10^{-2}$.

$$
n_S = \begin{cases}
\dfrac{1}{2}\cos\psi, & \text{for } \lambda_{c1} \ll \lambda_c, \\[2mm]
\dfrac{\pi}{2}\dfrac{\lambda_c}{L}\cos^2\psi, & \text{for } \lambda_{c2} \ll \lambda_c \ll \lambda_{c1}, \\[2mm]
\dfrac{\pi}{2}\dfrac{\lambda_m^2}{L\lambda_c}, & \text{for } \lambda_{c3} \ll \lambda_c \ll \lambda_{c2}, \\[2mm]
\dfrac{\pi}{2}\dfrac{\lambda_c}{L}, & \text{for } \lambda_c \ll \lambda_{c3},
\end{cases}
\tag{51}
$$

respectively, with

$$
\lambda_{c1} = \frac{L}{\pi\cos\psi}, \quad \lambda_{c2} = \frac{\lambda_m}{\cos\psi}, \quad \lambda_{c3} = \lambda_m. \tag{52}
$$

Scaling laws for plasma production are immediate and similar to those of Eq. (51).

Figures 7(a) and 7(b) illustrate about the variation of plasma production with ψ and λ_c, and the parametric regions for each of the regimes. At normal incidence, the RSC regime coincides with the collisional one (since the Chodura

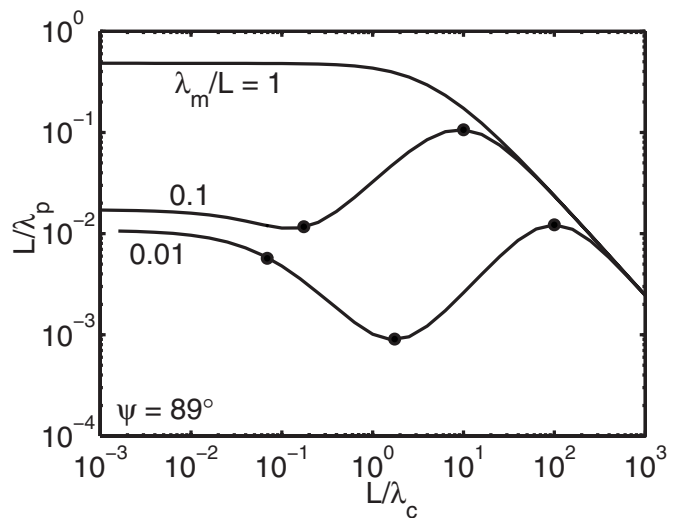layer vanishes) and the scaling laws of Self and Ewald are recovered. There are only mild changes in the parametric regions of the collisionless and RSC regimes within the oblique incidence range, Fig. 7(b). In fact, the DSC regime becomes a distinguished one only for grazing incidence, when it moves the parametric regions of the two other magnetized regions to lower collisionalities. Plasma dynamics at the two semicollisional regimes (at grazing incidence) present the similarities and differences commented in the previous section for the thin layer of near-parallel incidence and the Chodura layer.

Figure 8 shows the effect of the magnetic strength on plasma production at grazing incidence and illustrates on the extinction of the magnetized regimes at weak magnetic fields. As λ_m/L increases, the collisional regime occupies part of the interval in λ_c of the semicollisional regimes. The dashed lines of Fig. 3 show the effect of plasma collisionality on the velocity field for large incidence ($\psi=75°$): for non-zero collisionality, this provides some perpendicular diffusion and an increment of the $E\times B$ drift; when collisionality becomes large magnetic effects are progressively screened, the $E\times B$ drift vanishes, and the ion flux becomes perpendicular to the wall.

Equation (51) shows that plasma production presents local extrema at $\lambda_c=\lambda_{c2}$ and $\lambda_c=\lambda_{c3}$; plasma collection at these two extrema differ largely (in a ratio of about $\cos^{-1}\psi$) at grazing incidence and high magnetization. Indeed, plasmas with very *different* collisionalities and the *same* incidence angle can achieve the *same* wall-collected flux (and same total potential fall through the plasma). For instance, take the case of $\lambda_m/L=10^{-4}$ and $\cos\psi=10^{-2}$ ($\psi=89.4°$). Regime transitions are at $L/\lambda_{c1}\sim\pi\times10^{-2}$, $L/\lambda_{c2}\sim10^2$, and $L/\lambda_{c3}\sim10^4$, with plasma collections n_S about 10^{-2}, 10^{-6} (a local minimum), and 10^{-4} (a local maximum), respectively. Then, plasmas with L/λ_c equal to 10, 10^3, and 10^5 (within the RSC, DSC, and collisional regimes, respectively) have the same plasma collection, $n_S\simeq(\pi/2)\times10^{-5}$. However, the behavior of the velocity vector is very different. For instance, at point

S: v_{yS} and v_{zS} are $O(1)$ for $L/\lambda_c=10$; $v_{yS}=O(1)$ and $v_{zS}\ll 1$ for $L/\lambda_c=10^3$; and v_{yS} and v_{zS} are negligible for $L/\lambda_c=10^5$.

VI. FURTHER CONSIDERATIONS

A. On an experimental case

Harbour and Loarte,[20] studied the plasma collection at a tokamak limiter with grazing incidences between 88.8° and 89.7° and concluded that the ion velocity at the Chodura–Debye sheath edge of the limiter was subsonic. This would violate the Chodura condition and make impossible the matching with the Chodura–Debye sheath. Their conclusion is based on using

$$N_C V_{\parallel C} \equiv N_C V_{xC} \cos^{-1} \psi = N_C C_S v_C, \qquad (53)$$

$$N_C = N_M (1 + v_C^2)^{-1} \qquad (54)$$

[see Eq. (3) of their paper]. Measurements of magnitudes equivalent to our T, $N_C V_{\parallel C}$, and N_M, applied to these equations led them to conclude that $v_C < 1$ (down to $v_C \approx 0.25$ in one case). Equation (53) is correct for a magnetically aligned flux but Eq. (54) is valid only for the collisionless regime; it yields $N_C/N_M = 1/2$ for $v_C = 1$, as Eq. (23) does for $L/\lambda_c = 0$. The alternative conclusion, compatible with $v_C = 1$ and the matching with the Chodura–Debye sheath, is that Eq. (54) overestimates the plasma density (up to four times) at edge C. For an angle $\psi = 89.7°$ (i.e., $\cos \psi \approx 0.005$), the collisionless assumption supporting Eq. (54) requires a very low collisionality (compared to L): $\lambda_c > L_{\parallel}/4 = 50L$. Instead, were $200\lambda_m < \lambda_c < 50L$, the plasma would operate in the RSC regime, where the expression for the density ratio (satisfying $v_C = 1$) is

$$N_C = N_M (\pi \lambda_c / 2L) \cos \psi. \qquad (55)$$

This expression yields $N_C/N_M = 1/8$ for $\lambda_c \simeq 0.08 L_{\parallel}$. In Ref. 20 $L_{\parallel}$ seems to be about 1–3 m.

B. Nonzero Debye-length effects

Although in Sec. II the zero-Debye-length limit was defined in terms of the Debye length at the median M, Eq. (30) pointed out that the relevant Debye length for a distinguished Debye sheath is $\lambda_{dS} = \lambda_{dM} n_S^{-1/2}$ (to avoid confusions, $\lambda_{dM} \equiv \lambda_d$ is used here). Therefore, the correct zero-Debye-length limit is

$$n_S^{-1/2} \lambda_{dM} / \lambda_m \to 0. \qquad (56)$$

For grazing incidence, condition (56) is a much more restrictive condition than $\lambda_{dM}/\lambda_m \to 0$. Notice that in an unmagnetized plasma, nonzero Debye-length effects appear when $n_S^{-1/2} \lambda_{dM}$ is not small compared to λ_c, instead of λ_m, and then, the bulk region continues regularly into a collisional sheath. In the collisionless and RSC regimes of a magnetized plasma, it is the Chodura and Debye sheath that first merge in a single *collisionless* Chodura–Debye sheath. The details of this sheath are discussed in Appendix.

The simulations of Devaux and Manfredi show a decrease of the Mach number at edge S when ψ increases.[14] The arbitrariness in the definition of point S for a nonzero

Debye length is a possible explanation to it. An alternative explanation would rely on the possible anisotropy of the pressure tensor, which would yield a ψ-dependence of the temperature perpendicular to the wall.

VII. CONCLUSIONS

An asymptotic and parametric analysis has been carried out on a fluid model of a zero-Debye-length, source-driven plasma interacting with a wall and a magnetic field oblique to it, for a wide range of plasma collisionalities. In the distinguished zero-Debye-length, zero-Larmor-radius double limit and nonparallel magnetic incidence the plasma is structured as a magnetically aligned bulk region, a Chodura layer, and a Debye sheath. The sonic Chodura and Bohm conditions apply always at the singular region transitions. The Chodura layer is always source-free, collisionless, and independent of the plasma production model. Depending on plasma collisionality, the magnetically aligned bulk region evolves from collisionless to collisional, reproducing the structure of the unmagnetized presheath of the Self–Ewald model.

An asymptotic matched quasineutral solution has been derived for near-parallel incidence, consisting of a bulk diffusive-collisional region and a thin convective layer, with a sonic transition between them. Similarities and differences of that thin layer and the Chodura layer are stood out in the main text. The case of parallel incidence is acknowledged to require an extended model that includes electron dynamics and perpendicular transport.

A Tonks–Langmuir balance condition determines the plasma production and the wall-collected flux, in terms of the angle incidence and two length-scale ratios measuring magnetic strength (i.e., ion Larmor radius) and plasma collisionality. A detailed investigation has been carried out in terms of these input parameters, unveiling four different regimes. There is first the collisionless regime, where plasma production is the only mechanism driving the plasma in the magnetically aligned bulk region, and magnetic drifts dominate the intermediate Chodura layer. Then, there is the resistive semicollisional regime, where collisions retard the plasma transport in the magnetically aligned bulk region. At larger collisionalities, there is the diffusive semicollisional regime, where plasma dynamics change appreciably: in the bulk region the $E \times B$ drift is dominant, complemented by a diffusive wall-perpendicular flux; this last flux becomes convective and accelerates rapidly in a thin quasineutral layer. Finally, there is the collisional regime, where magnetic effects are completely cancelled out by collisions and ions flow perpendicularly to the wall. The diffusive semicollisional regime is distinguishable clearly at grazing incidence only. The collisionless regime disappears practically at near-parallel incidence.

Asymptotic scaling laws for wall-collected flux are given for the four regimes and any incidence angle. It is noteworthy that this flux does not vary monotonically with plasma collisionality (at a given angle of incidence). The dominance of either the resistive (i.e., retardation of B-parallel transport) or the diffusive (i.e., enhancement of

B-perpendicular transport) character of ion collisions determines the plasma transport in each of the two semicollisional regimes. The plasma flux to the wall presents a local minimum at the transition between the two semicollisional regimes and a local maximum at the transition between the diffusive semicollisional and the collisional regimes. These extrema become very pronounced at grazing incidence and high magnetization.

Finally, at very oblique incidence the large fall of plasma density across the plasma can bring up nonzero Debye-length effects that blur the Debye sheath edge. Then, for a weakly collisional plasma and large magnetic incidence, the Chodura and Debye sheaths merge in a single magnetized non-neutral region, which does not admit a simple solution.

ACKNOWLEDGMENTS

APPENDIX: NONZERO DEBYE LENGTH EFFECTS

When condition (56) is not well satisfied, non-neutral effects appear before the wall-perpendicular velocity becomes sonic and the Debye sheath edge, point *S*, becomes blurred. In the three-region structure of a strongly magnetized plasma, the first distinguished limit for studying this problem is

$$\frac{\lambda_m}{L}, \frac{\lambda_m}{\lambda_c} \ll 1, \quad \frac{\lambda_{dS}}{\lambda_m} \equiv \frac{\lambda_{dM}}{\lambda_m}(n_C \cos \psi)^{-1/2} = O(1), \quad \text{(A1)}$$

when the plasma structure consists of a magnetically aligned bulk region and a Chodura–Debye *single* sheath (in contrast to the Chodura–Debye *double* sheath for $\Lambda_{dm} \equiv \lambda_{dS}/\lambda_m \equiv \to 0$). The pertinent (source-free and collisionless) equations for that single sheath are

$$\frac{\lambda_{dM}^2}{\lambda_m^2}\frac{d^2\phi}{d\zeta^2} = \exp\frac{\phi}{t_e} - \frac{n_C \cos \psi}{v_x}, \quad \text{(A2)}$$

$$(v_x - t_i/v_x)dv_x/d\zeta = v_y \sin \psi - d\phi/d\zeta, \quad \text{(A3)}$$

$$v_x dv_y/d\zeta = v_z \cos \psi - v_x \sin \psi, \quad \text{(A4)}$$

$$v_x dv_z/d\zeta = -v_y \cos \psi. \quad \text{(A5)}$$

These equations conserve the mechanical energy and the magnetically aligned momentum:

$$v^2/2 + \phi + t_i \ln n_i = \text{const}, \quad \text{(A6)}$$

$$n_C v_\| + n_i t_i + n_e t_e - \frac{1}{2}\left(\frac{\lambda_{dM}}{\lambda_m}\frac{d\phi}{d\zeta}\right)^2 = \text{const}, \quad \text{(A7)}$$

but these expressions are not enough to reduce the problem to a single quadrature. Integration is further hindered when $\cos \psi < \sqrt{t_i}$ because Eq. (A3) presents a singularity at $v_x = \sqrt{t_i}$, which is removed by imposing that the right-hand side of Eq. (A3) is zero there. The wall potential fall across the Chodura–Debye sheath, Φ_{WC}, still satisfies condition (34).

The Chodura–Debye single sheath was discussed by Ahedo.[12] He showed, first, that the single sheath equations require the fulfillment of the Chodura condition $v_C \geq 1$ too. Therefore, Eq. (23) provides the boundary conditions to apply at the edge *C*. Second, for $\cos \psi < \sqrt{t_i}$, the solution near *C* consists of two fundamental modes, which are linearly combined in order to make regular the crossing of $v_x = \sqrt{t_i}$. Third, in all cases, the solution combines characteristics of ion-cyclotron and space-charge modes. Fourth, as Λ_{dm} increases, the velocity field in the plane of incidence tends to be magnetically aligned, whereas the out-of-plane drift, v_y, is maximum for $\Lambda_{dm} \sim 1$. For $\Lambda_{dm} \gg 1$, the plasma is magnetically aligned in the sheath and the solution is analytical. And fifth, the ion energy at the wall (i.e., $v_W^2/2$) is practically insensitive to Λ_{dm}, but the angle of impact decreases with Λ_{dm}, thus modifying possible wall sputtering.

[1]C. Pitcher and P. Stangeby, Plasma Phys. Controlled Fusion **39**, 779 (1997).
[2]R. Boswell and F. Chen, IEEE Trans. Plasma Sci. **25**, 1229 (1997).
[3]M. Martínez-Sánchez and J. Pollard, J. Propul. Power **14**, 688 (1998).
[4]L. Tonks and I. Langmuir, Phys. Rev. **34**, 876 (1929).
[5]D. Bohm, *The Characteristics of Electrical Discharges in Magnetic Fields* (MacGraw-Hill, New York, 1949), p. 77.
[6]S. Self, J. Appl. Phys. **36**, 456 (1965).
[7]R. Bissell, P. Johnson, and P. Stangeby, Phys. Fluids B **1**, 1133 (1989).
[8]J. Scheuer and G. Emmert, Phys. Fluids B **2**, 445 (1990).
[9]S. Self and H. Ewald, Phys. Fluids **9**, 2486 (1966).
[10]R. Chodura, Phys. Fluids **25**, 1628 (1982).
[11]K. Riemann, Phys. Plasmas **1**, 552 (1994).
[12]E. Ahedo, Phys. Plasmas **4**, 4419 (1997).
[13]R. Chodura, Contrib. Plasma Phys. **32**, 219 (1992).
[14]S. Devaux and G. Manfredi, Phys. Plasmas **13**, 083504 (2006).
[15]K. Riemann, Contrib. Plasma Phys. **34**, 127 (1994).
[16]R. Franklin, J. Phys. D **38**, 3412 (2005).
[17]T. Zimmermann, M. Coppins, and J. Allen, Phys. Plasmas **15**, 072301 (2008).
[18]N. Sternberg and J. Poggie, IEEE Trans. Plasma Sci. **32**, 2217 (2004).
[19]D. Sharma and H. Ramachandran, Phys. Rev. E **66**, 026412 (2002).
[20]P. Harbour and A. Loarte, Nucl. Fusion **35**, 759 (1995).
[21]E. Ahedo and D. Carralero, Bull. Am. Phys. Soc. **51**, 346 (2006).